Resonant tunneling through GaAs quantum-well energy levels confined by $Al_xGa_{1-x}As$ Γ- and X-point barriers

A. R. Bonnefoi and T. C. McGill
Thomas J. Watson, Sr. Laboratory of Applied Physics, California Institute of Technology, Pasadena, California 91125

R. D. Burnham*
Xerox Corporation, Palo Alto Research Center, Palo Alto, California 94304
(Received 30 November 1987)

Resonant tunneling is investigated in $GaAs/Al_xGa_{1-x}As$ double-barrier heterostructures grown by metal-organic chemical-vapor deposition (MOCVD) in the [100] direction. The quantum-well energy levels which produce the negative differential resistances observed in the experimental current-voltage characteristics are identified by calculating the energy-band diagrams of the structures. Energy-band profiles are essential to properly account for the voltage drops in all the layers, and to correlate unambiguously the experimental negative differential resistances with the resonances in the well. In samples having pure AlAs barrier layers, the peaks in current correspond to resonant states confined in the GaAs well by the AlAs X-point potential-energy barriers in addition to the AlAs Γ-point barriers. The quasibound X states are associated with the large longitudinal effective mass in AlAs corresponding to the direction perpendicular to the heterojunction interfaces. The relative intensity of Γ- and X-point tunneling is found to differ from sample to sample. In some structures, it also depends on the sign of the applied bias. Such effects may be related to the quality of the materials and the heterojunction interfaces.

I. INTRODUCTION

Resonant tunneling structures featuring two $Al_xGa_{1-x}As$ quantum barriers separated by a GaAs quantum well are extensively studied, both theoretically and experimentally.[1-8] In most studies, the barrier layers are made of direct-band-gap $Al_xGa_{1-x}As$ alloys ($x < 0.40-0.45$). As a result, resonant tunneling occurs via quasistationary states in the GaAs quantum well which are bound by the $Al_xGa_{1-x}As$ Γ-point potential-energy barriers. Even when $Al_xGa_{1-x}As$ is indirect, it is often assumed that the symmetry point to consider in the barriers should be the Γ point. However, recent experimental and theoretical studies have indicated that indirect-band-gap tunneling could be important in heterostructures in which the barrier layers are made of indirect-band-gap materials.[9-11]

This paper presents a study of resonant tunneling through $GaAs/Al_xGa_{1-x}As$ double-barrier heterostructures grown in the [100] direction by metal-organic chemical-vapor deposition (MOCVD). For each sample discussed, the quasistationary energy levels in the GaAs quantum well which produce the negative differential resistances observed in the experimental current-voltage (I-V) characteristics are identified. This is achieved by calculating the energy-band diagrams of the heterostructure. Energy-band profiles are important to determine the actual shapes of the potential-energy barriers through which the electrons tunnel. Furthermore, they give the voltage drop distributions not only in the quantum barriers and well but also in the cladding layers. These distributions may differ significantly from those based on the usual assumption that the entire applied voltage drops linearly across the barriers and well. As a result, energy-band diagrams are essential in finding the positions of the resonant states in the quantum well and in determining the origin of the peaks in current obtained in the experimental I-V curves.

Section II presents the theoretical approach by which the energy-band profiles of resonant tunneling double-barrier heterostructures are calculated and used to identify the resonances producing the experimental negative differential resistances. In Sec. III the validity of this approach is discussed in the case of structures having direct-band-gap $Al_xGa_{1-x}As$ barrier layers. In Sec. IV the model is applied to two samples with pure AlAs quantum barriers. Some of the negative differential resistances observed in the experimental I-V characteristics of both structures are found to be inconsistent with resonant states in the well bound by the AlAs Γ-point potential-energy barriers. However, they can be accounted for by considering tunneling via resonances confined by the AlAs X-point potential energy barriers. In Sec. V results obtained for two other samples with AlAs barrier layers are presented. These structures serve to illustrate that the relative contributions to the total current of tunneling via states bound by the AlAs Γ and X minima may depend upon the samples studied. Finally, the results of this study are summarized in Sec. VI.

The structure parameters of the five samples discussed in this paper are summarized in Table I. All of the samples were grown by MOCVD on [100]-oriented n^+-GaAs substrates. A first epitaxial layer of degenerate GaAs, doped n type with Se, was grown 2–3 μm thick. This layer was followed by two thin layers of $Al_xGa_{1-x}As$ or

TABLE I. Structure parameters.

Sample	Barrier composition	Barrier and well thicknesses (Å) Left barrier	Well	Right barrier	Doping densities (cm^{-3}) Left electrode (Se)	Right electrode (Se)	Barriers (Mg)
A	$Al_{0.35}Ga_{0.65}As$	59.5	51	59.5	1.2×10^{18}	1.2×10^{18}	2×10^{17}
B	AlAs	85	45	71	1.5×10^{18}	1.3×10^{18}	6×10^{17}
C	AlAs	42	62	51	1.75×10^{18}	1.75×10^{18}	6×10^{17}
D	AlAs	37	28.5	48	1.5×10^{18}	1.5×10^{18}	6×10^{17}
E	AlAs	71	76.5	79	4.7×10^{17}	5×10^{17}	2×10^{17}

pure AlAs, separated by a thin layer of GaAs forming the quantum well. Finally, a GaAs top layer was grown, degenerately doped with Se. The GaAs well was nominally undoped. The quantum barriers were doped *p* type with Mg. The layer thicknesses were determined from transmission electron microscopy measurements. This information was important because resonant energy levels can be highly sensitive to quantum well thicknesses, particularly for samples with very thin wells. For example, the calculated lowest Γ bound state for sample *D* (see Tables I and II) shifts by 40 meV if the well thickness is reduced by one monolayer. On the other hand, samples with thicker quantum wells, such as sample *A*, show shifts of less than 5 meV for variations of one monolayer. Electrode doping densities were obtained from Polaron doping profiles. Barrier doping concentrations were estimated from the flow rates used during growth. They could thus be in error due to background doping and dopant memory effects and to the difficulty of accurately calibrating ultrathin layer doping levels. This uncertainty could produce variations of up to 20 mV in calculated *I-V* peak positions if the calibrated doping concentrations are in error by a factor of 5. Circular devices, 20–250 μm in diameter, were prepared on the epitaxial sample faces using conventional photolithography, metallization, and etching techniques.[9]

II. THEORETICAL MODEL

The theoretical approach used to calculate the energy-band diagrams of resonant tunneling heterostructures is similar to that reported elsewhere for single-barrier tunnel structures.[12] Energy-band profiles are obtained by solving Poisson's equation in the direction perpendicular to the heterojunction interfaces. A major approximation is made in that neither the two-dimensional energy subbands in accumulation layers nor the quasistationary states in the quantum well are solved for self-consistently along with the energy-band edges. This avoids the complexity of calculating proper bound charge distributions. Although self-consistent calculations have been reported,[13–15] it is not clear whether or not they yield resonant peak positions which differ significantly from those obtained with "simple" band bending models. Once the band edges and the voltage drops have been determined in each layer, the resonant states in the quantum well are found in the quasiclassical approximation.[16] In this approach, the transfer-matrix technique for a general potential energy function $E_p(x)$ is used to calculate the transmission coefficient for resonant tunneling through the double-barrier heterostructures. The energies of the quasistationary states in the quantum well are then determined implicitly from the condition for resonance:

$$\int_a^b k(x)dx = \arctan\left[\frac{m_w^*\rho_l(a)}{m_l^*k(a)}\right] + \arctan\left[\frac{m_w^*\rho_r(b)}{m_r^*k(b)}\right] + (n-1)\pi\ , \quad n=1,2,3,\ldots, \qquad (1)$$

where

$$k(x)\equiv\{(2m_w^*/\hbar^2)[E-E_p(x)]\}^{1/2}$$

TABLE II. Theoretical and experimental voltages corresponding to peaks in current in the *I-V* characteristics.

Sample	Resonance	Reverse bias: V_p^R (mV) Theoretical	Experimental	Forward bias: V_p^F (mV) Theoretical	Experimental
A	E_1^Γ	−255	−255	255	255
B	E_1^X	−200	−200	240	240
	E_1^Γ	−480	−480	530	530
C	E_1^X	−140	−140	135	135
	E_1^Γ	−250	−250	240	240
	E_2^X	−750	−750	650	650
D	E_1^Γ	−1100	−1100	830	840
E	E_1^X	−100		90	90
	E_1^Γ	−190	−190	175	
	E_2^X	−450		420	420

denotes the electron wave vector in the well,

$$\rho_i(x) \equiv \{(2m_i^*/\hbar^2)[E_p(x)-E]\}^{1/2}$$

is the attenuation constant in barrier i, a and b correspond to the classical turning points in the quantum well at the energy E of the tunneling electron, and the subscripts l and r indicate the left and right barriers, respectively.

When the barrier layers are made of direct-band-gap alloys, it is expected that quantum well states which are bound by the $Al_xGa_{1-x}As$ Γ-point potential-energy barriers will yield the dominant resonant tunneling effects. However, for large-Al compositions ($x>0.40$–0.45), $Al_xGa_{1-x}As$ becomes indirect, and three sets of resonant states should be considered. First, these states may be quasistationary levels confined by the $Al_xGa_{1-x}As$ Γ-point potential-energy barriers. Other quasistationary levels of interest are those which are confined by the $Al_xGa_{1-x}As$ X-point potential-energy barriers and correspond to the large longitudinal X-point electron mass in $Al_xGa_{1-x}As$. These levels should be considered because the breaking of translational symmetry in the direction perpendicular to the interfaces allows $Al_xGa_{1-x}As$ X-point states to couple to GaAs Γ-point states.[9] Finally, there could be tunneling via states which are bound by the $Al_xGa_{1-x}As$ X-point potential-energy barriers and correspond to the small transverse X-point effective mass in $Al_xGa_{1-x}As$. These levels should be considered if electrons are allowed to scatter into virtual states beneath the four $Al_xGa_{1-x}As$ X valleys lying along the k_y and k_z directions, parallel to the planes of the interfaces.[9]

Once the energy-band diagrams and the quasistationary levels in the GaAs well have been calculated using the simple model described above, it becomes possible to identify the resonances giving rise to the negative differential resistances observed in the experimental I-V characteristics. This is particularly useful in determining the nature of the dominant-current transport mechanisms taking place in double-barrier heterostructures.

III. STRUCTURES WITH DIRECT $Al_xGa_{1-x}As$ BARRIER LAYERS

The validity of the approach presented in Sec. II may be discussed in the case of structures having direct-band-gap $Al_xGa_{1-x}As$ barrier layers. In this instance, the resonant tunneling current through the lower energy Γ-point barriers is expected to be much larger than that through the X-point barriers.

Sample A is a double-barrier heterostructure having $Al_{0.35}Ga_{0.65}As$ quantum barriers. These barriers are 59.5 Å thick (21 monolayers), and their p-type doping concentration is estimated to be 2×10^{17} cm^{-3}. The GaAs electrodes are degenerately doped n type with Se at 1.2×10^{18} cm^{-3}. The nominally undoped GaAs quantum well is 51 Å wide (18 monolayers). Figure 1 depicts an experimental I-V characteristic at 4.2 K for a circular device, 50 μm in diameter. One negative differential resistance appears in each bias direction. The peak currents correspond to applied voltages of ±255 mV. The valley

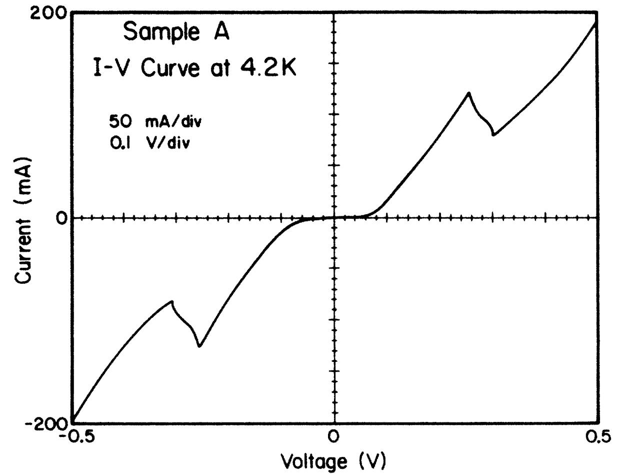

FIG. 1. Experimental I-V characteristic at 4.2 K for a circular device, 50 μm in diameter, fabricated on a GaAs/$Al_{0.35}Ga_{0.65}As$ double-barrier heterostructure (sample A). The GaAs electrodes are degenerately doped n type with Se at 1.2×10^{18} cm^{-3}. The 59.5-Å-thick barrier layers are doped p type with Mg at 2×10^{17} cm^{-3}. The nominally undoped GaAs quantum well is 51 Å wide.

currents occur at about ±300 mV. The inflections observed in the regions with negative slopes arise from the difficulty of performing stable curve tracer measurements of negative differential resistances. For the structures discussed in this paper, reverse bias ($V_a<0$) corresponds to a negative voltage applied to the top GaAs electrode with respect to the substrate. Figures 2(a) and 2(b) show calculated conduction-band edges for the same heterostructure under applied biases of -60 and -255 mV, respectively. In GaAs ($Al_{0.35}Ga_{0.65}As$), the low temperature band gap is assumed to be 1.52 eV (1.96 eV), the effective mass is taken to be $0.067m_0$ ($0.096m_0$), and the relative dielectric constant is 13.18 (12.05).[17] A valence-band discontinuity of $0.55x$ eV is assumed at GaAs-$Al_xGa_{1-x}As$ interfaces,[18] resulting here in a conduction-band offset of 245 meV. Using these values, two resonant states are found in the GaAs quantum well in the unbiased structure. Their energies, measured from the conduction-band edge at the middle of the well, are $E_1^\Gamma=73$ meV for the ground state, and $E_2^\Gamma=242$ meV for the first excited state. At low applied voltages ($|V_a|<60$ mV) E_1^Γ remains above the Fermi energy E_f^i in the incident electrode, and the current is very small. As shown in Fig. 2(a), E_1^Γ coincides in energy with E_f^i when $|V_a|=60$ mV. At this point, resonant tunneling via E_1^Γ is initiated.[19] As $|V_a|$ becomes larger, more electrons may tunnel resonantly via E_1^Γ, and the current increases rapidly. The peak in the I-V curve should occur when the applied voltage becomes large enough to cause the conduction-band edge in the negatively biased electrode to line up with E_1^Γ. Figure 2(b) indicates that this occurs when $|V_a|=255$ mV. The results predicted by the energy-band diagrams are thus in excellent agreement with the experimental data shown in Fig. 1. They are summarized in Table II. In fact, this agreement is

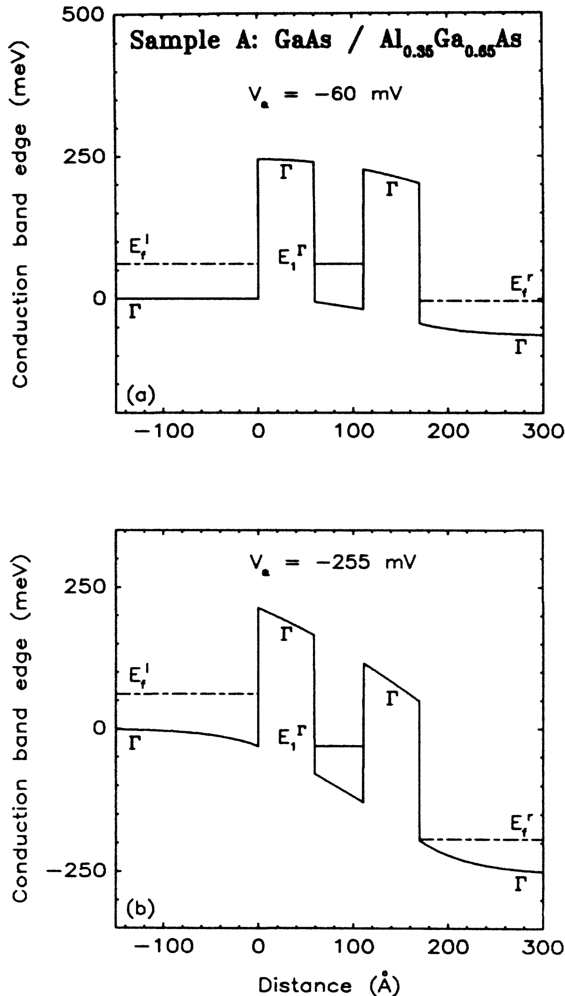

FIG. 2. Calculated Γ-point conduction-band edges as functions of distance in the direction perpendicular to heterojunction interfaces for the same heterostructure as in Fig. 1 (sample A). (a) and (b) Applied biases of -60 and -255 mV, respectively. The Fermi level in the left (right) GaAs electrode is E_f^l (E_f^r). The conduction-band discontinuity at the heterojunction interfaces is taken to be 245 meV. E_1^{Γ} denotes the first resonant state in the quantum well confined by the $Al_{0.35}Ga_{0.65}As$ Γ-point potential-energy barriers.

surprisingly good considering the simplifying assumptions used in calculating the energy-band profiles and the uncertainties within which the band offsets and the barrier doping densities are known.

The energy-band diagrams depicted in Fig. 2 reveal that the shapes of the band edges may deviate significantly from those obtained when band bending is neglected. In particular, an accumulation layer adjacent to the first heterojunction interface is formed in the negatively biased electrode when enough voltage is applied. It follows that the number of incident electrons increases with $|V_a|$. Furthermore, if $E_c^b(x=0)$ denotes the barrier conduction-band edge at $x=0$, then

$$\Delta E_{\text{eff}} \equiv E_c^b(x=0) - E_f^i ,$$

the effective conduction-band offset for electrons tunneling near the Fermi energy E_f^i, is a decaying function of $|V_a|$. When band bending is ignored, the bands remain flat in the cladding layers, ΔE_{eff} is constant, and the number of incident electrons is independent of V_a. The resonant states in the well, the tunneling transmission coefficients, and the theoretical I-V curves calculated using these two approaches are thus expected to be different. For example, if band bending is neglected and the entire applied voltage is assumed to drop linearly across the barriers and the well in the heterostructure illustrated in Figs. 1 and 2, resonant tunneling via E_1^{Γ} should be initiated at about ± 25 mV instead of ± 60 mV. Similarly, the peaks in current should occur at approximately ± 150 mV and not at ± 255 mV. This demonstrates that band-bending effects and cladding layer voltage drops are important in interpreting the experimental results.

The energy-band profiles depicted in Fig. 2 indicate further that negative differential resistances are obtained when $E_c^i(x=0)$, the conduction-band edge in the incident electrode at the first heterojunction interface coincides in energy with the quasistationary states in the quantum well. In fact, two-dimensional energy subbands exist in accumulation layers, and the peaks in current should occur when the resonances in the well line up with the lowest two-dimensional subband. However, the GaAs electrodes in the heterostructures studied are usually heavily doped. Consequently, the accumulation layers are not very large, and the role of subband levels is reduced. Furthermore, as long as the resonances are not too high in energy, the negative differential resistances are obtained at reasonably low applied biases, and the accumulation layer in the incident electrode remains small. As a result, the error introduced by neglecting the two-dimensional subbands should not be significant. This is the case in Fig. 2(b). For high-energy states in the well, this error is expected to become larger. The fact that the peaks in current occur when the quasistationary levels in the GaAs well coincide in energy with $E_c^i(x=0)$ may also be due to band-tailing effects in the degenerately doped electrodes. These effects are difficult to evaluate quantitatively. Nevertheless, because electronic states exist in the cladding layers right below the conduction-band edges, the peaks in current may actually occur when these states line up with the resonances in the quantum well. Band-tailing effects may also be related to the widths of the negative differential resistances observed in the I-V characteristics.

Other samples having direct $Al_xGa_{1-x}As$ barrier layers were studied using the same approach. Equally good agreement was found between the experimental I-V curves and the quasibound Γ states in the well provided the energy-band diagrams of the heterostructures were used. This confirms the importance of taking into account the voltage drops in all the layers and the actual shapes of the band edges. Energy-band profiles should thus be essential in interpreting the experimental results obtained from samples having indirect-band-gap $Al_xGa_{1-x}As$ barrier layers, and in which the tunneling mechanisms are more complex than in structures with direct $Al_xGa_{1-x}As$ quantum barriers.

IV. STRUCTURES WITH AlAs BARRIER LAYERS

In this section the same model is applied to GaAs/AlAs double-barrier heterostructures. In sample *B* the doping densities in the GaAs electrodes are slightly asymmetric: 1.5×10^{18} cm^{-3} in the top cladding layer and 1.3×10^{18} cm^{-3} in the electrode adjacent to the substrate. The nominally undoped GaAs well is 45 Å wide (16 monolayers). The *p*-type doping concentration in the AlAs layers is estimated to be 6×10^{17} cm^{-3}. The AlAs barrier closer to the substrate is 71 Å thick (25 monolayers). The other barrier is 85 Å thick (30 monolayers). This asymmetry in barrier thicknesses should cause a given resonance in the well to be manifested at a larger applied voltage in forward bias than in reverse bias ($|V_a^F| > |V_a^R|$). Figure 3 shows an experimental *I-V* characteristic at 4.2 K for a circular device, 50 μm in diameter. Two weak negative differential resistances exist in each bias direction. In forward bias, the peaks in current occur at $V_1^F=240$ mV and $V_2^F=530$ mV. In reverse bias, they take place at $V_1^R=-200$ mV and $V_2^R=-480$ mV. The *I-V* curve also reveals that resonant tunneling is initiated at approximately ±100 mV. To calculate the resonant states in the well confined by the AlAs Γ-point potential-energy barriers, the effective mass in AlAs is taken to be $m_\Gamma^*=0.15m_0$,[17] and the conduction-band offsets at the heterojunction interfaces are assumed to be 1.0 eV.[18] Using these values, two quasibound Γ states are found in the unbiased structure, at energies $E_1^\Gamma=125$ meV and $E_2^\Gamma=517$ meV above the conduction-band edge at the middle of the well. To obtain the states confined by the AlAs *X*-point potential-energy barriers, the conduction-band offsets are assumed to be 0.19 eV.[18] When the large longitudinal *X*-point electron mass $m_{X_l}^*=1.1m_0$ is used in the barriers, one quasistationary state $E_1^X=30$ meV is found in the GaAs well. The level associated with the small transverse electron mass $m_{X_t}^*=0.19m_0$ has an energy $\varepsilon_1^X=59$ meV from the bottom of the well. Two energy-band profiles for the structure are depicted in Fig. 4. They correspond to reverse biases of -200 and -480 mV, respectively. Both Γ- and *X*-point conduction-band edges are shown in the AlAs barriers.

If quasibound Γ states alone are considered, the resonances of importance are E_1^Γ and E_2^Γ. These lie 125 and 517 meV above the conduction-band edge at the middle of the well in the unbiased structure. If band bending is neglected and the entire applied voltage is assumed to

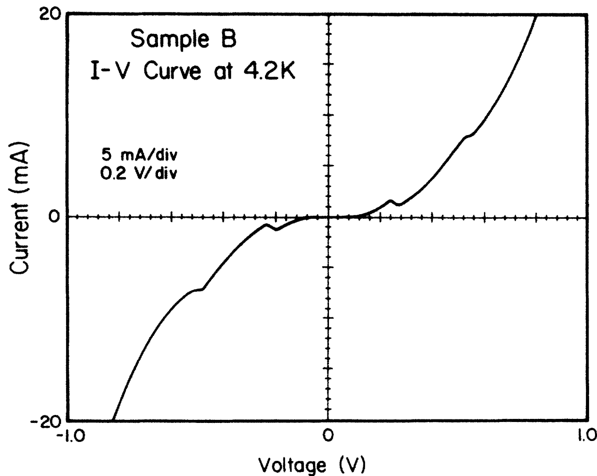

FIG. 3. Experimental *I-V* characteristic at 4.2 K for a circular device, 50 μm in diameter fabricated on sample *B*. Sample *B* is a GaAs/AlAs double-barrier heterostructure in which the nominally undoped GaAs quantum well is 45 Å wide. The doping densities in the *n*-type GaAs electrodes are 1.5×10^{18} cm^{-3} in the top cladding layer and 1.3×10^{18} cm^{-3} in the electrode adjacent to the substrate. The barrier layers are doped *p* type with Mg at 6×10^{17} cm^{-3}. The AlAs barrier closer to the substrate is 71 Å thick. The other barrier is 85 Å thick.

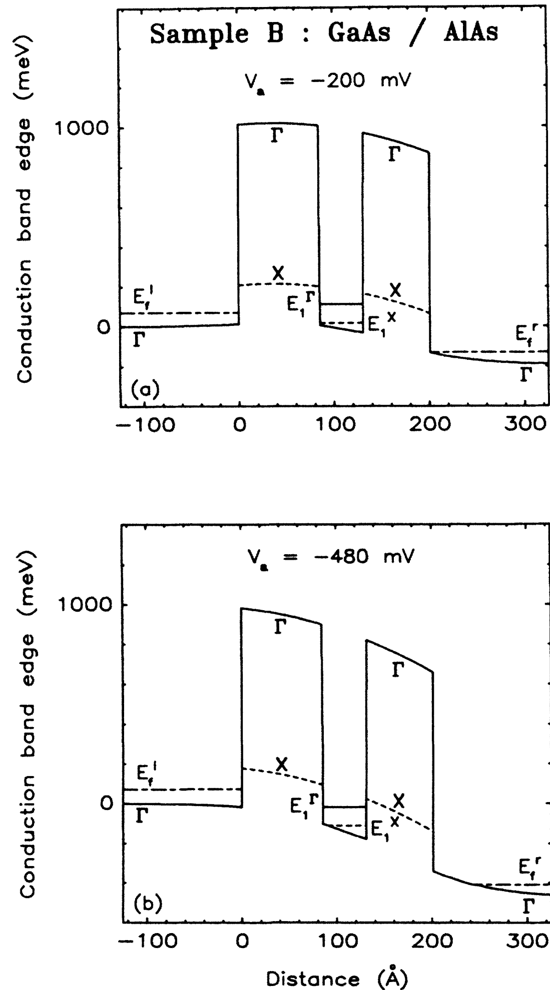

FIG. 4. Calculated Γ-point (solid lines) and *X*-point (dashed lines) conduction-band edges, for the same heterostructure as in Fig. 3 (sample *B*). (a) and (b) Applied biases of -200 and -480 mV, respectively. The conduction-band discontinuities at the heterojunction interfaces are 1.0 eV at the Γ point and 0.19 eV at the *X* point. In the GaAs quantum well E_1^Γ (solid line) denotes the first quasibound Γ state, and E_1^X (dashed line) is the resonant *X* state corresponding to the large longitudinal AlAs *X*-point electron mass in the direction perpendicular to the interfaces.

drop linearly across the quantum barriers and well, the peaks in current corresponding to E_1^Γ should occur in the I-V curves at about ± 250 mV. This could be consistent with the negative differential resistances observed at -200 and 240 mV in Fig. 3. However, E_2^Γ should appear in the I-V characteristics at voltages $|V_a| > 1$ V. This is in disagreement with the experimental results. If band bending is taken into account, the cladding layers sustain part of the applied bias. This reduces the amount of voltage dropping across the quantum barriers and well. As a result, the disagreement with the experimental data becomes even larger than when band bending is neglected. It may thus be concluded that resonant tunneling via quasibound Γ states alone is inconsistent with the sample I-V characteristics. However, the energy-band diagram illustrated in Fig. 4(b) indicates that in reverse bias, E_1^Γ lines up with $E_c^l(x=0)$ when $V_a = -480$ mV. Similarly, energy-band profile calculations predict that the peak in current due to E_1^Γ should occur in forward bias at $V_a = 530$ mV. These values correspond precisely to the negative differential resistances observed in Fig. 3 at V_2^R and V_2^F, respectively. The peaks in current at $V_1^R = -200$ mV and $V_1^F = 240$ mV may then correspond to a quasistationary X state. Figure 4(a) reveals that E_1^X coincides in energy with $E_c^l(x=0)$ when $V_a = -200$ mV. Similarly, the peak in current associated with E_1^X is anticipated in forward bias at $V_a = 240$ mV. Energy-band diagrams also indicate that resonant tunneling via E_1^X should be initiated at -90 and 110 mV in reverse and forward bias, respectively. These results are in good agreement with the experimental data. The negative differential resistances obtained in the I-V characteristics of sample B thus correspond to E_1^X, the quasistationary X state associated with the large longitudinal X-point effective mass in the AlAs barriers and E_1^Γ, the lower quasibound Γ state. This is summarized in Table II. Figure 3 reveals further that the two negative differential resistance regions obtained in each bias direction are comparable in size. This indicates that both resonances are equally important in current transport through sample B. It will be shown in Sec. V that the relative contributions to the total current of resonant tunneling via quasistationary Γ and X states may actually depend upon the structures studied.

These concepts are further illustrated on another double-barrier heterostructure with pure AlAs barrier layers. In sample C the GaAs electrodes are doped n type at 1.75×10^{18} cm^{-3}. The nominally undoped GaAs quantum well is 62 Å wide (22 monolayers). As in sample B, the AlAs layers are doped p type at 6×10^{17} cm^{-3}. The barrier closer to the substrate is 51 Å thick (18 monolayers), whereas the one adjacent to the top electrode is only 42 Å thick (15 monolayers). Figure 5 shows an experimental I-V characteristic at 4.2 K for a circular device, 20 μm in diameter. The I-V curve reveals that the first peaks in current occur at $V_1^F = 135$ mV in forward bias, and $V_1^R = -140$ mV in reverse bias. Other resonances appear at 650 and -750 mV. The temperature dependence of the device I-V curves may be used to tentatively interpret the shapes of the broad negative differential resistances observed at $|V_a| < 280$ mV. At

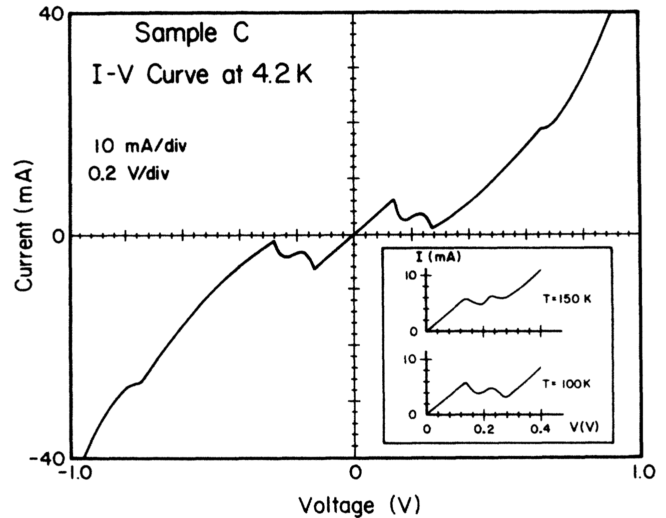

FIG. 5. Experimental I-V characteristic at 4.2 K for a circular device, 20 μm in diameter, fabricated on sample C. Sample C is a GaAs/AlAs double-barrier heterostructure in which the nominally undoped GaAs quantum well is 62 Å wide. The GaAs electrodes are doped n type with Se at 1.75×10^{18} cm^{-3}. The AlAs barrier layers are doped p type with Mg at 6×10^{17} cm^{-3}. The barrier closer to the substrate is 51 Å thick. The barrier adjacent to the top electrode is 42 Å thick.

room temperature, inflections are visible at about ± 140 mV. As the temperature T is decreased, the low-voltage regions of the I-V curves ($|V_a| < 140$ mV) remain almost identical, while the background current decays rapidly for larger values of $|V_a|$. As a result, the negative differential resistances become more pronounced. When $T \approx 200$ K, two new small peaks appear at about ± 240 mV, next to the existing peaks at ± 140 mV. As T is further reduced, all the peaks become more prominent. This temperature dependence is illustrated in the insert of Fig. 5. It should be mentioned that the I-V characteristics of other devices prepared on the same sample do not reveal two such distinct current peaks in each bias direction at $|V_a| < 280$ mV, but only one broad negative differential resistance region. These adjacent peaks may thus be due to two resonant states in the quantum well which are close enough in energy that they are not always resolved in the I-V curves.

The energy-band diagrams of the heterostructure and the quasistationary levels in the GaAs well may be calculated as for sample B. Three quasibound Γ states are found at energies $E_1^\Gamma = 78$ meV, $E_2^\Gamma = 325$ meV, and $E_3^\Gamma = 730$ meV in the unbiased structure. The two resonant X states corresponding to the large longitudinal AlAs X-point mass lie at energies $E_1^X = 22$ meV and $E_2^X = 165$ meV above the bottom of the well. The quasistationary X states associated with the small transverse AlAs X-point mass have energies $\varepsilon_1^X = 42$ meV and $\varepsilon_2^X = 176$ meV from the conduction-band edge at the middle of the well. It could be argued that if band-bending effects are neglected, the experimental results are consistent with resonant tunneling via the quasibound Γ

states E_1^Γ and E_2^Γ alone. However, since the AlAs barriers are doped p type to a significant level, the band edges actually bend up at zero bias. As a result, the bottom of the well and the resonant states are raised by about 50 meV with respect to the band edges in the bulk electrodes. Furthermore, it has been shown that the cladding layers sustain significant fractions of the applied voltage. When these two effects are taken into account, the experimental I-V curves are found to be inconsistent with resonant tunneling via Γ states alone. In reverse bias, energy-band profiles indicate that when $V_a=-140$ mV (-250 mV), E_1^X (E_1^Γ) coincides in energy with $E_c^l(x=0)$. In forward bias, the same would occur at 135 mV (240 mV). Comparing these values to the experimental results depicted in Fig. 5 suggests that the broad negative differential resistance regions observed in the I-V characteristics at $|V_a|<280$ mV arise from tunneling via the two resonant states E_1^X and E_1^Γ. Since the difference in energy between both levels is slightly smaller than the Fermi energy in the bulk electrodes, E_1^X and E_1^Γ are not always resolved. Energy-band diagrams indicate further that the small current peaks obtained in Fig. 5 at -750 and 650 mV are due to resonant tunneling via E_2^X. It may thus be concluded that the I-V characteristics of sample C reveal resonant tunneling via the first quasi-bound Γ state E_1^Γ and the two X states E_1^X and E_2^X, corresponding to the large longitudinal AlAs X-point effective mass. Energy-band profiles also make it possible to predict the voltages at which tunneling via each of the quasi-bound states in the well may be initiated. Since E_1^X lies below the Fermi level at zero bias, resonant tunneling via E_1^X starts as soon as a voltage is applied. Consequently, the experimental zero-bias resistance is small and the portions of the I-V curves corresponding to $|V_a|<140$ mV remain almost independent of temperature. Resonant tunneling via E_1^Γ (E_2^X) is initiated when E_1^Γ (E_2^X) coincides in energy with the Fermi level in the incident electrode. For both resonances, this occurs approximately when tunneling via the previous quasistationary state in the well turns off. Such effects would thus contribute in reducing the peak-to-valley current ratios of the negative differential resistances.

V. RELATIVE IMPORTANCE OF RESONANT Γ AND X STATES

In this section the model is applied to two other samples with pure AlAs barrier layers. These samples serve to illustrate that the relative contributions to the total current of the different mechanisms for tunneling through double-barrier heterostructures having indirect-band-gap $Al_xGa_{1-x}As$ quantum barriers may depend upon the structure studied.

As indicated in Table I, the GaAs electrodes in sample D are doped n type at 1.5×10^{18} cm^{-3}. The nominally undoped GaAs quantum well is 28.5 Å wide (10 monolayers). The p-type doping density in the AlAs barrier layers is estimated to be 6×10^{17} cm^{-3}. The barrier closer to the substrate is 48 Å thick (17 monolayers). The barrier adjacent to the top electrode is 37 Å thick (13 monolayers). Figure 6 shows an experimental I-V characteristic at 4.2 K for a circular device, 20 μm in diameter. The I-V curve reveals one region with negative slope in each bias direction. The peaks in current occur at $V_1^R=-1.1$ V in reverse bias, and $V_1^F=840$ mV in forward bias. Resonant tunneling is initiated at about -400 and 340 mV in reverse and forward bias, respectively. Four resonant energy levels are found in the unbiased structure at energies $E_1^X=47$ meV, $\varepsilon_1^X=90$ meV, $E_1^\Gamma=225$ meV, and $E_2^\Gamma=898$ meV above the conduction-band edge at the middle of the well. Energy-band diagram calculations indicate that resonant tunneling via E_1^Γ is initiated at -420 and 350 mV in reverse and forward bias, respectively. Similarly, the peaks in current corresponding to E_1^Γ are anticipated at -1.1 V and 830 mV. These results are summarized in Table II. They are in good agreement with the experimental data depicted in Fig. 6. It may thus be concluded that resonant tunneling via E_1^Γ is the dominant low-temperature current transport mechanism in sample D. Furthermore, as opposed to samples B and C, no sign of tunneling via resonant X states is visible in the I-V curves. This shows that the relative contributions to the total current of resonant tunneling via quasistationary Γ and X states in the GaAs well may differ from sample to sample.

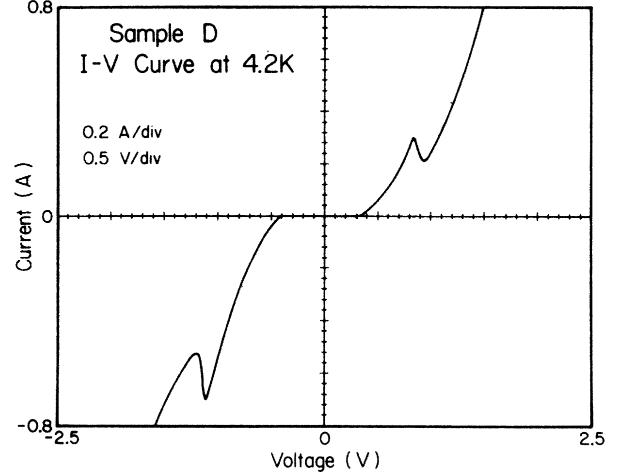

FIG. 6. Experimental I-V characteristic at 4.2 K for a circular device, 20 μm in diameter, fabricated on sample D. Sample D is a GaAs/AlAs double-barrier heterostructure in which the nominally undoped GaAs quantum well is 28.5 Å wide. The GaAs electrodes are doped n type with Se at 1.5×10^{18} cm^{-3}. The AlAs barrier layers are doped p type with Mg at 6×10^{17} cm^{-3}. The barrier closer to the substrate is 48 Å thick. The other barrier is 37 Å thick.

In sample E, the doping densities in the GaAs electrodes are slightly asymmetric: 4.7×10^{17} cm^{-3} in the top cladding layer and 5×10^{17} cm^{-3} in the electrode adjacent to the substrate. The nominally undoped GaAs well is 76.5 Å wide (27 monolayers). The p-type doping density in the AlAs barrier layers is estimated to be 2×10^{17} cm^{-3}. The AlAs barrier closer to the substrate is 79 Å thick (28 monolayers). The other barrier is 71 Å thick (25 monolayers). In this sample, the effects of the asymmetric barrier thicknesses are partially compensated

by the asymmetric electrode doping concentrations. Figure 7 is an experimental *I-V* characteristic at 4.2 K for a circular device, 80 μm in diameter. Only one negative differential resistance is observed in reverse bias. The corresponding peak in current occurs at −190 mV. In forward bias, two regions with negative slopes are obtained at $V_1^F = 90$ mV and $V_2^F = 420$ mV, respectively. The fact that the first peak in current appears in forward bias at an applied voltage as low as 90 mV indicates that the corresponding resonance is close to the bottom of the GaAs quantum well. The lowest four resonant energy levels calculated from the conduction-band edge at the middle of the well in the unbiased structure are $E_1^X = 17$ meV, $\varepsilon_1^X = 33$ meV, $E_1^\Gamma = 57$ meV, and $E_2^X = 120$ meV. Energy-band diagram calculations reveal that resonant tunneling via E_1^X, E_1^Γ, and E_2^X should be initiated in reverse (forward) bias at −40 (35), −110 (100), and −240 (200) mV, respectively. Similarly, the corresponding peaks in current should occur at −100, −190, and −450 mV in reverse bias, and at 90, 175, and 420 mV in forward bias. These results are also summarized in Table II. Thus, we conclude that the two negative differential resistances obtained at V_1^F and V_2^F in Fig. 7 correspond to tunneling via the resonant *X* states E_1^X and E_2^X. In reverse bias, the peak in current observed at −190 mV is consistent with resonant tunneling via E_1^Γ, but no quasibound *X* state is observed. These results reveal that the relative importance of tunneling via resonant Γ and *X* states not only differs from sample to sample, but may also depend upon the sign of the applied voltage.

Other samples studied using the same approach led to similar results and conclusions. These observations indicate that current transport is more complex in structures having indirect-band-gap $Al_xGa_{1-x}As$ barrier layers than in samples in which the quantum barriers are made of direct $Al_xGa_{1-x}As$ alloys. Numerous quasistationary states are then present in the quantum well, causing resonant tunneling to occur through multiple processes. This produces large background currents and reduced peak-to-valley current ratios. This also explains why certain resonances are not observed in experimental *I-V* characteristics and that expected negative differential resistances are totally absent in some samples. For the resonant states to be individually resolved, the Fermi levels in the bulk electrodes should be smaller than the energy spacing between the resonances. This may be achieved by reducing the well width and the electrode doping densities. However, the experimental results seem to suggest that the contributions of the different tunneling mechanisms to the total current may be more sensitive to the presence of defects, impurities and interface states than to layer thicknesses or doping concentrations.

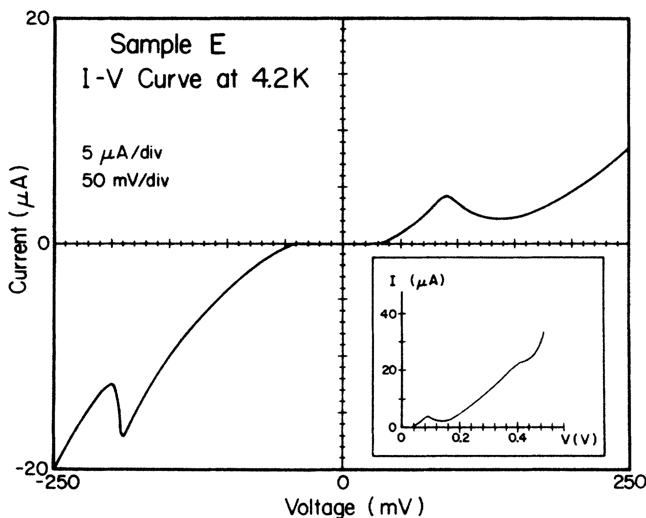

FIG. 7. Experimental *I-V* characteristic at 4.2 K for a circular device, 80 μm in diameter, fabricated on sample *E*. Sample *E* is a GaAs/AlAs double-barrier heterostructure in which the nominally undoped GaAs quantum well is 76.5 Å wide. The doping densities in the *n*-type GaAs electrodes are 4.7×10^{17} cm^{-3} in the top cladding layer and 5×10^{17} cm^{-3} in the electrode adjacent to the substrate. The barrier layers are doped *p* type with Mg at 2×10^{17} cm^{-3}. The AlAs barrier closer to the substrate is 79 Å thick. The other barrier is 71 Å thick.

VI. SUMMARY

The objective of the study presented in this paper was to identify the resonant energy levels in the GaAs quantum well producing negative differential resistances in the *I-V* characteristics of GaAs/$Al_xGa_{1-x}As$ double-barrier tunnel structures grown by MOCVD on [100]-oriented substrates. This provides useful information not only about the dominant tunneling processes occurring in these heterostructures, but also about their relative contributions to the total current. This was achieved by comparing the experimental *I-V* data to results obtained from the calculated energy-band diagrams of the heterostructures. The main results of this study may be summarized as follows. (i) Energy-band diagrams give the actual shapes of the potential-energy barriers through which the charge carriers tunnel. These shapes may differ significantly from those based on the usual assumption that the entire applied voltage drops linearly across the quantum barriers and well. (ii) Taking into account band-bending effects and the fractions of the applied bias sustained by the cladding layers is critical in obtaining good agreement between the positions of the quasistationary levels in the GaAs quantum well and the peaks in current observed in the experimental *I-V* curves. (iii) In samples having direct-band-gap $Al_xGa_{1-x}As$ barrier layers, the negative differential resistances arise solely from resonant tunneling via quasibound Γ states in the GaAs quantum well. The lack of observable tunneling current through the indirect barriers is probably caused by the relative energy positions of the Γ- and *X*-point minima when the barriers are made of direct-band-gap alloys. (iv) When the barrier layers are made of pure AlAs, tunneling via resonant Γ states alone is often inconsistent with the experimental *I-V* characteristics of the samples. (v) The experimental data may then usually be explained by tunneling via resonant states confined in the well by the AlAs *X*-point potential-energy barriers in addition to resonant tunneling via states bound by the AlAs Γ-point potential-energy barriers. (vi) The quasibound *X* states

are found to be associated with the large longitudinal X-point electron mass in AlAs and not with the small transverse effective mass. This reveals that tunneling through the indirect AlAs band gap arises primarily from the coupling of virtual AlAs X-point states with GaAs Γ-point states due to the breaking of translational symmetry in the direction perpendicular to the heterojunction interfaces. (vii) Mendez *et al.*[8] have suggested that resonant tunneling through confined states in the AlAs layer at the X point may explain I-V features which are not attributable to conventional Γ-point tunneling. However, this mechanism is clearly not responsible for the low-voltage features reporter here (i.e., those labeled E_1^X in Table II), since states confined in AlAs could only be reached with much higher voltages. Furthermore, we have demonstrated that the straightforward Γ-X-Γ-X-Γ mechanism also explains the higher voltage peaks observed here. (viii) The relative intensities of tunneling via Γ- and X-resonant states in the quantum well are found to vary from sample to sample. In some heterostructures these contributions also depend upon the sign of the applied bias. Such effects may be related to the quality of the materials and the heterojunction interfaces. However, it is not clear whether enhanced or decreased tunneling via X-bound states results from samples with fewer defects and sharper interfaces. (ix) The multiple processes by which electrons may tunnel through GaAs/AlAs resonant tunneling structures are consistent with the small peak-to-valley current ratios usually obtained from these samples.

ACKNOWLEDGMENTS

The authors wish to acknowledge R. S. Bauer, T. L. Paoli, D. H. Chow, and T. K. Woodward for valuable discussions and are grateful to H. F. Chung, F. J. Endicott, D. M. Taylor, T. T. Tjoe, F. A. Ponce, W. J. Mosby, D. W. Treat, and S. E. Nelson for technical assistance. This work was supported in part by the U. S. Defense Advanced Research Projects Agency under Contract No. N00014-84-C-0083 and the U. S. Office of Naval Research under Contract No. N00014-82-K-0556.

---

*Present address: Amoco Research Center, P.O. Box 400, Warrenville Road, Naperville, IL 60566.
[1]R. Tsu, and L. Esaki, Appl. Phys. Lett. **22**, 562 (1973).
[2]L. L. Chang, L. Esaki, and R. Tsu, Appl. Phys. Lett. **24**, 593 (1974).
[3]T. C. L. G. Sollner, W. D. Goodhue, P. E. Tannenwald, C. D. Parker, and D. D. Peck, Appl. Phys. Lett. **43**, 588 (1983).
[4]A. R. Bonnefoi, R. T. Collins, T. C. McGill, R. D. Burnham, and F. A. Ponce, Appl. Phys. Lett. **46**, 285 (1985).
[5]T. J. Shewchuk, P. C. Chapin, P. D. Coleman, W. Kopp, R. Fischer, and H. Morkoç, Appl. Phys. Lett. **46**, 508 (1985).
[6]M. A. Reed and J. W. Lee, Superlatt. Microstruct. **3**, 111 (1987).
[7]E. E. Mendez, W. I. Wang, B. Ricco, and L. Esaki, Appl. Phys. Lett. **47**, 415 (1985).
[8]E. E. Mendez, E. Calleja, C. E. T. Gonçalves da Silva, L. L. Chang, and W. I. Wang, Phys. Rev. B **33**, 7368 (1986).
[9]A. R. Bonnefoi, D. H. Chow, T. C. McGill, R. D. Burham, and F. A. Ponce, J. Vac. Sci. Technol. B **4**, 988 (1986).
[10]I. Hase, H. Kawai, K. Kaneko, and N. Watanabe, J. Appl. Phys. **59**, 3792 (1986).
[11]A. C. Marsh, IEEE J. Quantum Electron. **QE-23**, 371 (1987).
[12]A. R. Bonnefoi, D. H. Chow, and T. C. McGill, J. Appl. Phys. **62**, 3836 (1987).
[13]T. Ando, J. Phys. Soc. Jpn. **51**, 3893 (1982).
[14]H. Ohnishi, T. Inata, S. Muto, N. Yokoyama, and A. Shibatomi, Appl. Phys. Lett. **49**, 1248 (1986).
[15]Y. Rajakarunanayake and T. C. McGill, J. Vac. Sci. Technol. B **5**, 1288 (1987).
[16]B. Ricco and M. Ya. Azbel, Phys. Rev. B **29**, 1970 (1984).
[17]H. C. Casey and M. B. Panish, *Heterostructure Lasers, Part A* (Academic, New York, 1978), p. 192.
[18]J. Batey and S. L. Wright, J. Appl. Phys. **59**, 200 (1986).
[19]S. Luryi, Appl. Phys. Lett. **47**, 490 (1985).